Charge transfer and antiferromagnetic insulator phase in $SrRu_{1-x}Cr_xO_3$ perovskites: Solid solutions between two itinerant electron oxides

A. J. Williams, A. Gillies, and J. P. Attfield
Centre for Science at Extreme Conditions, University of Edinburgh, Erskine Williamson Building, King's Buildings, Mayfield Road, Edinburgh, EH9 3JZ, United Kingdom

G. Heymann and H. Huppertz
Department Chemie, Ludwig-Maximilians-Universität München, Butenandtstraße 5-13, 81377 München, Germany

M. J. Martínez-Lope and J. A. Alonso
Instituto de Ciencia de Materiales de Madrid, CSIC, Cantoblanco, 28049 Madrid, Spain
(Received 23 December 2005; revised manuscript received 24 January 2006; published 9 March 2006)

A full range of $SrRu_{1-x}Cr_xO_3$ perovskite solid solutions ($0<x<1$) has been prepared using high temperatures and pressures up to 10.5 GPa. The structure changes from orthorhombic *Pbnm* at low x through a previously unreported rhombohedral $R\bar{3}c$ phase at $x=0.4$ to cubic $Pm\bar{3}m$ for $0.5<x<1$. No Cr/Ru order is evidenced at any x. A substantial $Ru^{4+}+Cr^{4+}\rightarrow Ru^{5+}+Cr^{3+}$ charge transfer is evidenced by a volume discontinuity close to $x=0.5$. Low Cr-doped materials ($x<0.3$) are itinerant, and ferromagnetic below 160–190 K, and $x>0.7$ materials are itinerant and Pauli paramagnetic, but a substantial insulating region is found between these limits. Neutron diffraction shows the $x=0.4$ material to be antiferromagnetic with a high Néel temperature ~400 K and a saturated moment of $1.7\mu_B$, despite the large Cr/Ru disorder. A 50 K magnetic transition and a low temperature structural phase change to orthorhombic *Imma* symmetry have been discovered in $SrCrO_3$, suggesting that the ground state of this simple perovskite is more complex than was previously assumed.

DOI: 10.1103/PhysRevB.73.104409 PACS number(s): 75.30.Kz, 71.30.+h, 64.70.Kb, 61.66.−f

I. INTRODUCTION

Transition metal oxide perovskites are of enduring interest because of the properties that result from highly correlated *d*-band electrons and strong electron-lattice couplings. $SrRuO_3$ and $SrCrO_3$ are notable as both are intrinsic metallic conductors.

The electronic and magnetic properties of $SrRuO_3$ have been studied extensively.[1–3] Ferromagnetic order occurs below $T_c=163$ K with a substantial spin-polarization of the low-spin t_{2g}^4 Ru^{4+} electrons giving a saturated moment of $1.6\mu_B$.[4] An orthorhombic *Pbnm* symmetry superstructure is found at 300 K due to tilting of the RuO_6 octahedra. $SrCrO_3$ has not been investigated so heavily as high pressures are required to prepare this phase. The original study reported that $SrCrO_3$ is an undistorted cubic perovskite ($a_p=3.818$ Å) and is Pauli paramagnetic down to 4 K.[5] The resistivity remains metallic down to 4 K, with a low residual value of 10^{-5} Ω cm.

Solid solutions between $SrRuO_3$ and $SrCrO_3$ are of interest to discover whether itinerant electron behavior can be tuned between the two end members, or whether insulating phases result from Cr/Ru disorder and charge transfer. It has recently been reported that $SrRu_{1-x}Cr_xO_3$ solid solutions up to $x=0.15$ can be synthesized at ambient pressure and 1250–1370 °C.[6–8] Notably, this increases the Curie temperature up to $T_c=188$ K, whereas other substituents reduce the T_c of $SrRuO_3$.[6] This has been attributed to a double-exchange interaction between minority spin t_{2g}–band electrons, resulting from partial $Ru^{4+}+Cr^{4+}\rightarrow Ru^{5+}+Cr^{3+}$ charge transfer.[8] An $x=0.2$ sample was also prepared in the latter study at a pressure of 3 GPa, but $SrRu_{1-x}Cr_xO_3$ solid solutions with higher Cr contents have not been reported. Here we present an investigation of the entire $SrRu_{1-x}Cr_xO_3$ series using appropriate pressures to stabilize the high x samples. The variations of perovskite superstructure, magnetism, and electronic conductivity are presented.

II. EXPERIMENTAL

Ceramic precursors for nominal $SrRu_{1-x}Cr_xO_3$ compositions were prepared from stoichiometric mixtures of $SrCO_3$, RuO_2, and Cr_2O_3, pelleted and sintered at 950 °C in air for 12 h. Single perovskite phase samples were obtained by reheating samples with x up to 0.15 twice for 12 h at 1100 °C under flowing nitrogen. However, materials with $x>0.2$ required high pressure to stabilize perovskite phases.

$SrRu_{1-x}Cr_xO_3$ samples with $x=0.4$ and 0.6 were synthesized in a piston cylinder apparatus. 0.4 g of the prereacted oxides above were sealed in a 6 mm diameter gold capsule which was placed in a cylindrical graphite heater. The reaction was carried out at a pressure of 3.5 GPa at 1000 °C for 1 h after which the sample was quenched to room temperature and the pressure was subsequently released. Small (~10 mg) $x=0.5$, 0.8, and 1 samples were prepared using a Walker-type, multianvil pressure module.[9] Each sample was held in a cylindrical boron nitride crucible at the center of a precast MgO octahedron, and was compressed to 10.5 GPa by eight truncated tungsten carbide cubes. A cylindrical graphite resistance heater contacted by two molybdenum

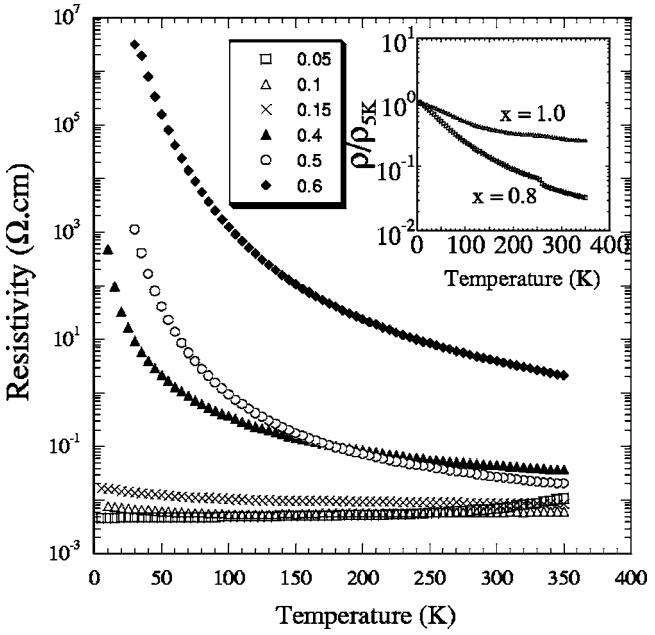

FIG. 1. Temperature-dependent resistivity measurements for sintered $SrRu_{1-x}Cr_xO_3$ materials, with x values indicated in the key. The inset shows the relative resistance variations for $x=0.8$ and 1 samples.

plates, was used to heat the sample to 1100 °C, and samples were cooled to ambient temperature before the pressure was released.

Powder x-ray diffraction patterns of all samples were recorded at room temperature using Cu$K_{\alpha 1}$ radiation. Powdered samples were also used for variable temperature SQUID magnetization measurements in a 500 Oe field between 4 and 320 K. Four probe resistance measurements were made on sintered bars between 4 and 350 K. Neutron diffraction data were collected on the constant wavelength diffractometer D20 at ILL, Grenoble, France, and on the GEM time-of-flight spectrometer at the ISIS spallation source, UK.

III. RESULTS

Three different lattice types were found for $SrRu_{1-x}Cr_xO_3$ perovskites as x changes from 0 to 1, and the properties of each group are described in the following sections.

A. $x=0-0.15$

These materials are very similar to those previously reported.[6–8] The samples have the orthorhombic *Pbnm* $\sqrt{2}a_p\times\sqrt{2}a_p\times 2a_p$ superstructure of $SrRuO_3$, and show an enhancement of T_c up to 188 K for $x=0.10$–0.15 samples. These materials are band ferromagnets, with saturated moments of $\sim 1\mu_B$/f.u., and they show metallic conductivity with little temperature dependence down to 4 K (Fig. 1).

B. $x=0.40$

This sample showed a different pattern of x-ray diffraction peak splittings compared to the low doped *Pbnm* and the higher x (cubic) materials (Fig. 2). The splittings from this previously unreported phase are consistent with a rhombohedral lattice distortion, and the x-ray data were fitted by an $R\bar{3}c$ symmetry perovskite superstructure model [$a=5.51909(4)$ and $c=13.4619(1)$ Å]. This structural distortion is known in other doped transition metal perovskites such as 30% doped $AMnO_3$ perovskites,[10] e.g., $La_{0.7}Sr_{0.3}MnO_3$.

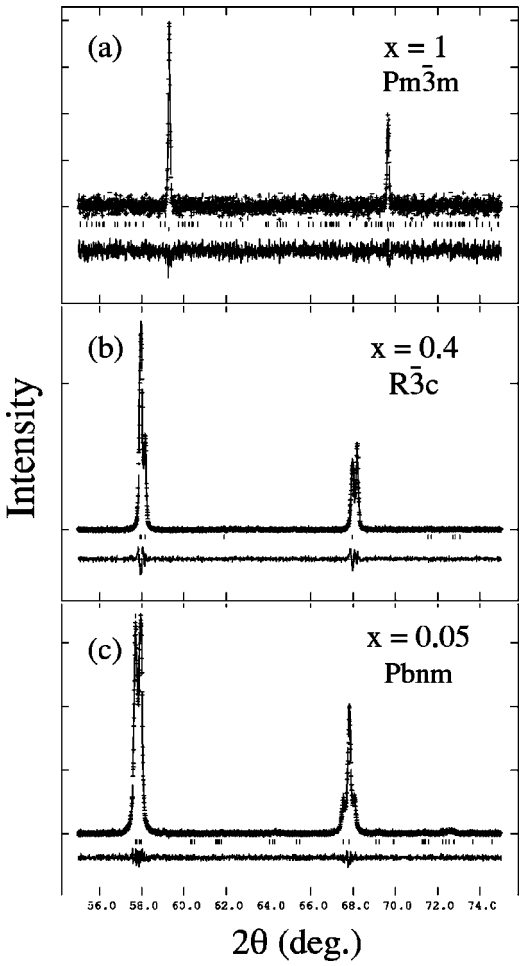

FIG. 2. Part of the $SrRu_{1-x}Cr_xO_3$ x-ray diffraction patterns for (a) $x=1$, cubic $Pm\bar{3}m$; (b) $x=0.4$, rhombohedral $R\bar{3}c$; and (c) $x=0.05$ orthorhombic *Pbnm*, showing the peak splittings associated with the different symmetries. Observed, calculated and difference profile intensities and the Bragg reflection markers are plotted.

Magnetization measurements between 4 and 320 K (Fig. 3) show a broad ferromagnetic transition with an onset at ~250 K for $SrRu_{0.6}Cr_{0.4}O_3$. The saturated moment of $\sim 0.15\mu_B$/f.u. (Fig. 4) is considerably less than that in the orthorhombic $x=0$–0.15 materials. This sample is also semiconducting (Fig. 1) showing that a metal-insulator boundary occurs in the $x=0.2$–0.4 region of the $SrRu_{1-x}Cr_xO_3$ phase diagram.

To investigate the structure and any magnetic order of the new rhombohedral phase $SrRu_{0.6}Cr_{0.4}O_3$, time-of-flight powder neutron diffraction profiles were recorded on the GEM diffractometer at ISIS between 4 and 300 K. Data from the detector banks at $2\theta=90°$, 64°, and 35° were Rietveld analyzed simultaneously using the GSAS suite.[11] Refinement of

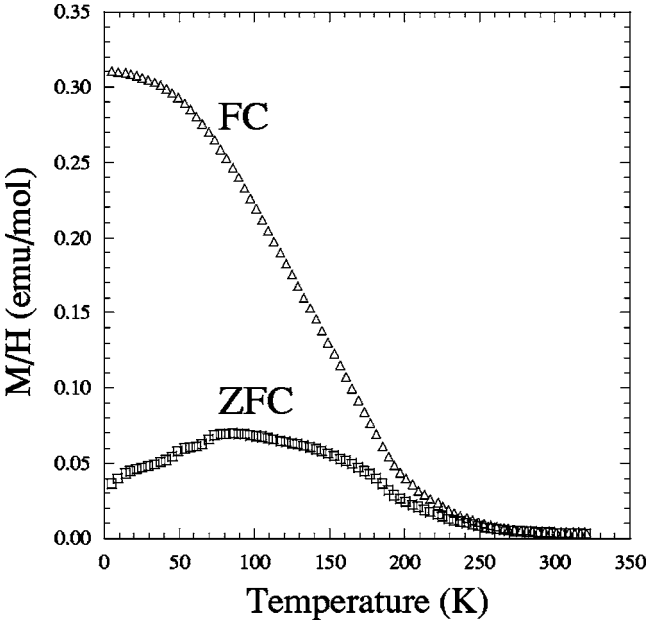

FIG. 3. Zero-field cooled (ZFC) and field-cooled (FC) magnetization measurements for $SrRu_{0.6}Cr_{0.4}O_3$ (x=0.4).

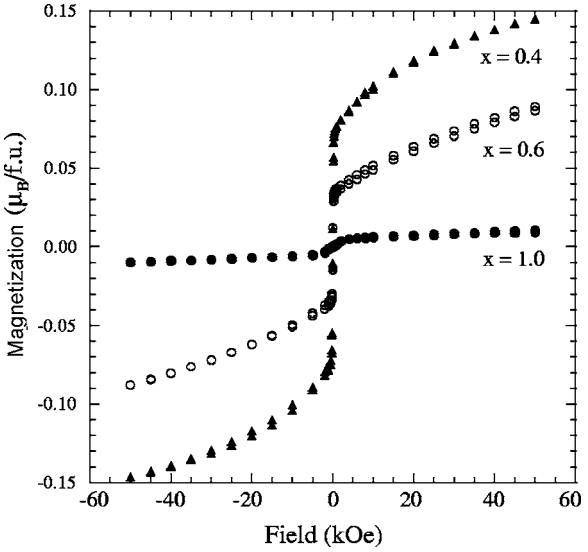

FIG. 4. Magnetization-field hysteresis plots for x=0.4, 0.6, and 1 $SrRu_{1-x}Cr_xO_3$ samples at 10 K.

the oxygen fractional occupancy showed the material to be stoichiometric to an experimental uncertainty of less than 1%. Lattice parameters, atomic coordinates and reliability factors are presented in Table I.

In addition to the peaks expected from the $R\bar{3}c$ superstructure of $SrRu_{0.6}Cr_{0.4}O_3$, a prominent (101) [cubic (1/2 1/2 1/2)] peak is also observed at all temperatures, diminishing slightly in intensity with increasing temperature (Fig. 5). Possible atomic or magnetic superstructures were explored by profile fitting. The (101) peak is not observed in the x-ray data, which rules out B-site Cr/Ru order as the origin of the superstructure, and other possible superstructures arising from oxygen displacements gave poor fits to the data, and physically unrealistic structures. However, this additional neutron diffraction peak is fitted well by a G-type antiferromagnetic model, in which moments at the Cr/Ru sites are antiparallel to the moments at all six neighboring sites. No other intense magnetic peaks are observed, or predicted by this model. Cr/Ru spins are parallel to the hexagonal c axis (equivalent to the [111] direction in rhombohedral or cubic settings). Magnetic order persists to the highest measured temperature of 300 K, and from the variation of the antiferromagnetically ordered moment (Fig. 6) we estimate that the ordering transition is ~400 K. The saturated moment of $1.7\mu_B$ per Cr/Ru is close to the predicted $2\mu_B$ for $S=1$ Ru^{4+}/Cr^{4+}, but could also be consistent with the ideal $3\mu_B$ for $S=3/2$ Ru^{5+}/Cr^{3+} in the charge transfer model described later, allowing for some moment reduction from disorder and covalency effects. The observation of a G-type spin ordering, with a high T_N and a substantial ordered moment shows that the M-O-M' interactions are antiferromagnetic for all M,M'=Cr,Ru combinations, so the system is not magnetically frustrated despite being substitutionally dis-

TABLE I. Refined cell and structural parameters (isotropic thermal displacement factors U_{iso}, Cr/Ru magnetic moment and O:x coordinate), Cr/Ru-O distances and reliability factors for $SrRu_{0.6}Cr_{0.4}O_3$ in space group $R\bar{3}c$ at temperatures 10 to 300 K. Atom positions Sr(6a)(0,0,1/4); Cr/Ru (6b)(0,0,0); O (18e)(x,0,1/4).

		10 K	50 K	100 K	150 K	200 K	250 K	300 K
a	(Å)	5.5171(1)	5.5173(1)	5.5178(1)	5.5185(1)	5.5196(1)	5.5209(1)	5.5225(1)
c	(Å)	13.4305(2)	13.4316(2)	13.4348(2)	13.4406(2)	13.4475(2)	13.4560(2)	13.4657(2)
Sr	U_{iso} (Å^2)	0.0034(1)	0.0035(1)	0.0038(1)	0.0045(1)	0.0052(1)	0.0061(1)	0.0067(1)
Cr/Ru	U_{iso} (Å^2)	0.0007(1)	0.0006(1)	0.0008(1)	0.0007(1)	0.0009(1)	0.0011(1)	0.0012(1)
	μ_z (μ_B)	1.71(3)	1.64(2)	1.65(2)	1.61(3)	1.51(3)	1.42(3)	1.32(3)
O	x	0.4683(1)	0.4685(1)	0.4687(1)	0.4695(1)	0.4702(1)	0.4711(1)	0.4719(1)
	U_{iso} (Å^2)	0.0060(1)	0.0061(1)	0.0063(1)	0.0066(1)	0.0071(1)	0.0077(1)	0.0083(1)
Cr/Ru-O	(Å)	1.954(1)	1.954(1)	1.955(1)	1.955(1)	1.955(1)	1.955(1)	1.956(1)
R_{wp}	(%)	7.58	7.05	7.00	7.05	7.07	7.08	7.04
χ^2		2.02	2.51	2.33	2.22	2.15	2.10	2.01

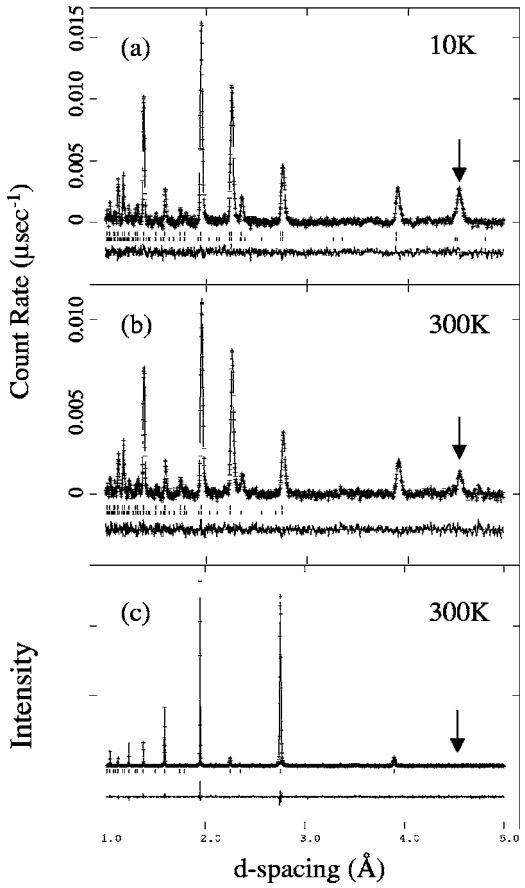

FIG. 5. Powder diffraction intensities for $SrRu_{0.6}Cr_{0.4}O_3$ plotted against d spacing for comparison; time-of-flight neutron patterns at (a) 10 K and (b) 300 K; (c) 300 K x-ray data. The cubic (1/2 1/2 1/2) superstructure reflection position is arrowed on each profile. Rietveld fits calculated from the structural $R\bar{3}c$ model and, in (a) and (b), the G-type spin structure are shown.

ordered. The antiferromagnetic interactions result from π-superexchange through $M:t_{2g}$-O:$2p-M':t_{2g}$ orbital pathways.

The structure of $SrRu_{0.6}Cr_{0.4}O_3$ remains rhombohedral down to 4 K and no anomalies in the lattice parameters (Fig. 7) or the atomic coordinates and distances (Table I) are evident. There is thus no structural evidence for a low temperature $R\bar{3}c \rightarrow Pbnm$ structural transition. The Cr/Ru-O bond length shows only a slight thermal expansion. The separation between the reduced hexagonal cell parameters decreases slightly with increasing temperature (Fig. 7), but any $Pm\bar{3}m \rightarrow R\bar{3}c$ transition (at which the reduced parameters converge) is clearly $\gg$300 K. As no structural distortion or additional magnetic scattering appears on cooling below 300 K, the ~250 K ferromagnetic transition that dominates the magnetization curve (Fig. 3) is likely to result from the presence of some orthorhombic, low x material, rather than being intrinsic to the antiferromagnetic insulating phase. However no secondary orthorhombic phase is resolved in the profile fits, suggesting that the ferromagnetic phase is poorly crystallized, in keeping with the broad magnetization transition.

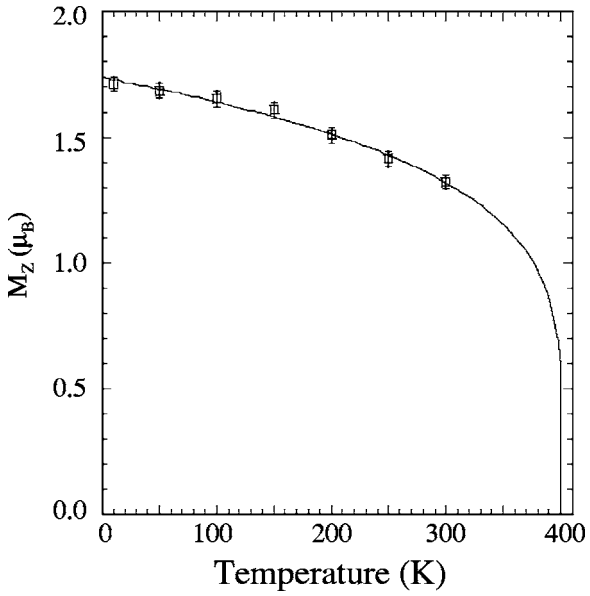

FIG. 6. Temperature variation of the antiferromagnetically ordered Cr/Ru moment in $SrRu_{0.6}Cr_{0.4}O_3$ (x=0.4) between 4 and 300 K. The line shows a critical law fit for a Néel transition estimated at ~400 K.

C. x=0.5–1

The materials in this range were all found to have undistorted, cubic $Pm\bar{3}m$ perovskite cells [a=3.88861(3), 3.88250(2), 3.84910(7), and 3.81844(6) Å, for x=0.5, 0.6, 0.8, and 1, respectively]. The x=0.5 material was prepared to investigate whether a "Sr_2CrRuO_6" double perovskite analog of Sr_2FeMoO_6 (Ref. 12) could be made. However, no x-ray superstructure peaks characteristic of Cr/Ru cation order are observed, so we conclude that this composition is a solid solution with no significant long-range cation order, as was also found for the rhombohedral x=0.4 sample above.

The x=0.5 and x=0.6 samples are semiconducting with resistivities comparable to the rhombohedral x=0.4 material

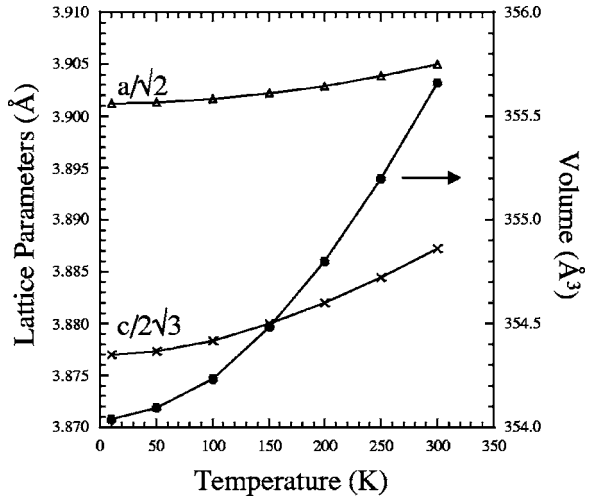

FIG. 7. Temperature variation of the normalized lattice constants (hexagonal setting) and cell volume of rhombohedral $SrRu_{0.6}Cr_{0.4}O_3$ (x=0.4) between 4 and 300 K. The lines are a guide to the eye.

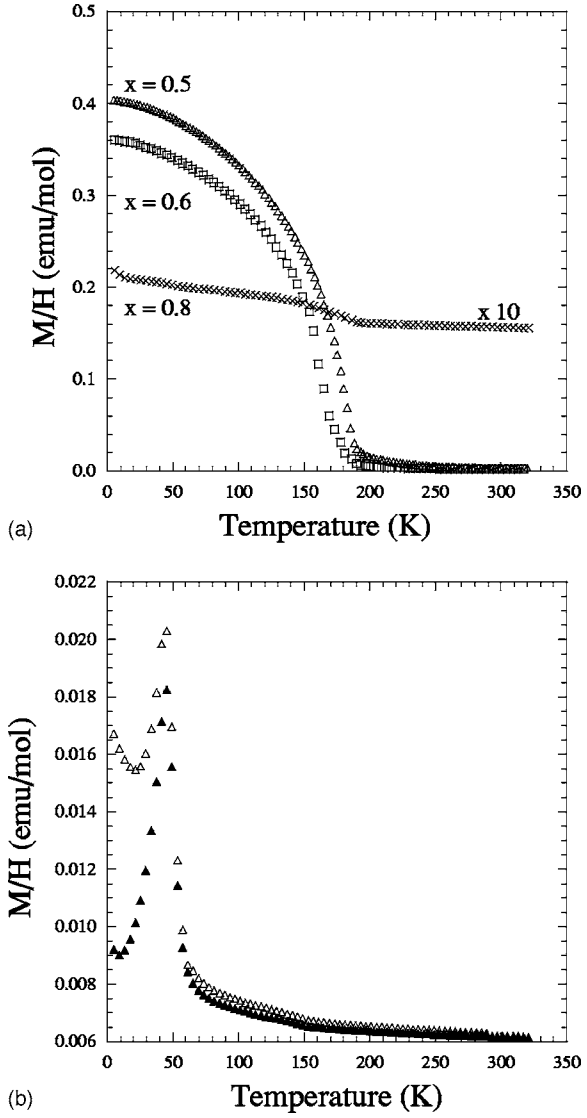

FIG. 8. Magnetization measurements for $SrRu_{1-x}Cr_xO_3$; (a) field-cooled data for $x=0.5$, 0.6, and 0.8 (the latter are multiplied by 10 for clarity), (b) $x=1$, showing zero-field cooled (filled triangles) and field-cooled (open triangles) data.

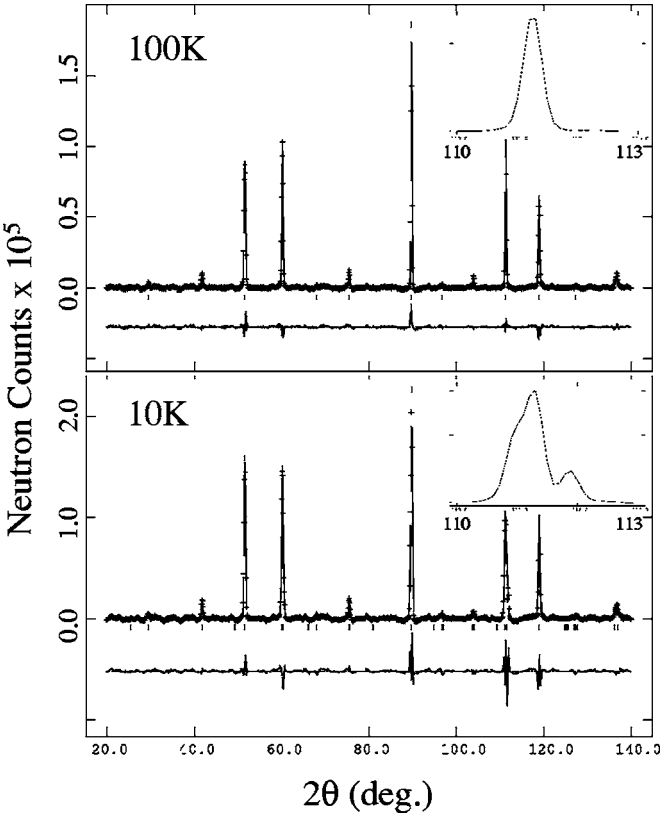

FIG. 9. Powder neutron diffraction patterns (wavelength 1.8885 Å) for $SrCrO_3$ at 100 and 10 K (with a background of 2.5 $\times 10^5$ counts subtracted). Insets show the cubic (311) peak, which splits into at least three components at 10 K.

(Fig. 1). It was difficult to measure the magnitude of resistivities for the small polycrystalline $x=0.8$ and 1 samples. However, the temperature variations of the sample resistances (inset of Fig. 1) show that both samples are metallic, as reported previously for $SrCrO_3$.[5] Hence, a second insulator-metal transition occurs in the $x=0.6$–0.8 interval of the $SrRu_{1-x}Cr_xO_3$ system.

Magnetization measurements in the 4–320 K range show an apparent ferromagnetic transition at 190 K [Fig. 8(a)] for the $x=0.5$, 0.6, and 0.8 samples, but not for $x=1$. The saturation moments are small ($<0.1\mu_B$/f.u.) and decrease with increasing x (Fig. 4). As this transition coincides with the upper limit of T_c for the low x orthorhombic samples, we conclude that it arises from Ru rich regions resulting from slight sample inhomogeneity, rather than being intrinsic to the cubic $x>0.5$ region. A further transition at 50 K is observed in the $x=0.8$ sample, and is prominent in the magnetization curve for $SrCrO_3$ [Fig. 8(b)]. This was not reported in the previous study of the latter phase.[5]

To clarify the low temperature properties of $SrCrO_3$, powder neutron diffraction profiles of a 20 mg sample (made by combining the products of two runs from the Walker cell) were recorded at 10 and 100 K on ILL diffractometer D20. The 100 K data show that the symmetry remains cubic [$a=3.8120(1)$ Å] down to this temperature, with no additional scattering evident (Fig. 9). The prominent peak splittings in the lowest temperature profile demonstrate that a structural phase transition occurs between 10 and 100 K. The splitting of the cubic (311) peak into at least three components (Fig. 9) shows that the symmetry is lower than rhombohedral. A satisfactory fit to the profile was obtained with a $\sqrt{2}a_p \times 2a_p \times \sqrt{2}a_p$ *Imma* superstructure, however, other low symmetry possibilities cannot be excluded and more highly resolved diffraction data will be needed to confirm this model. The results of the *Imma* refinement (Table II) show that the CrO_6 octahedra have a slight tetragonal compression at 10 K. This lattice distortion may relieve a Fermi surface instability in the cubic phase arising from the degeneracy of t_{2g}^2 Cr^{4+}.

No magnetic diffraction peaks are evident in the 10 K neutron diffraction profile of $SrCrO_3$ (Fig. 9), showing that no ordering of localized ($\sim 2\mu_B$) Cr^{4+} moments occurs between 100 and 10 K. The 50 K magnetic transition in $SrCrO_3$ therefore appears to be to a weakly ferromagnetic

TABLE II. Refined atomic parameters and Cr-O distances for the *Imma* phase of $SrCrO_3$ at 10 K. The lattice parameters are $a=5.3997(3)$, $b=7.6052(3)$, $c=5.3944(3)$ Å.

Atom	Site	x	y	z	U_{iso} (Å^2)
Sr	4*e*	0	0.25	0.001(11)	0.0043(7)
Cr	4*b*	0	0	0.5	0.0043(7)
O(1)	4*e*	0	0.25	0.499(14)	0.012(2)
O(2)	8*g*	0.25	0.492(1)	0.25	0.0060(7)
Cr-O(1)(Å)×2		1.901(1)			
Cr-O(2)(Å)×4		1.909(1)			

itinerant state; a small population difference between up and down spin states at the Fermi surface could result from the structural distortion. Further work will be needed to determine whether the magnetic and structural transitions coincide, and to detect any subtle magnetic order below 50 K, but the ground state of $SrCrO_3$ already appears to be more complex than the cubic Pauli paramagnetic phase reported previously.[5]

IV. DISCUSSION

This study has revealed the evolution of structural, magnetic and conducting properties across the $SrRu_{1-x}Cr_xO_3$ system, which shows several interesting new physical regimes. The structural evolution is from the *Pbnm*, $SrRuO_3$-type perovskite superstructure at low x to the undistorted cubic aristotype structure for $x=0.5$–1, via a rhombohedral phase observed at $x=0.4$ (Fig. 10). This $Pm\bar{3}m \rightarrow R\bar{3}c \rightarrow Pbnm$ sequence of phase transitions is found in other perovskite systems, e.g., manganites,[10] as the tolerance factor is reduced, but it may also be coupled to the changes between electronic phases.

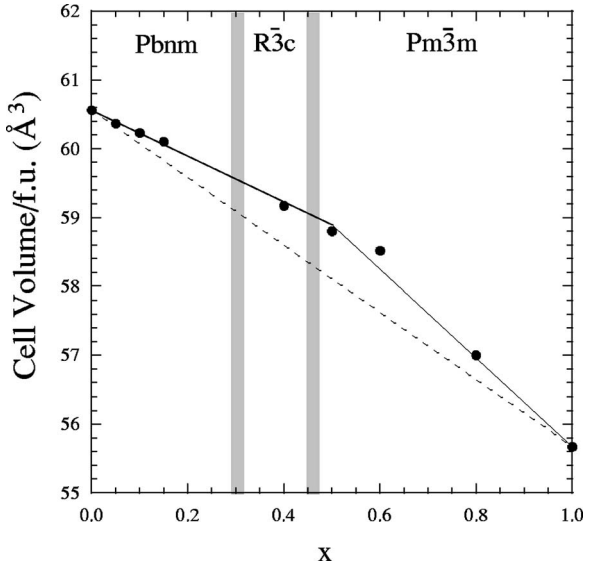

FIG. 10. Variation of the cell volume per unit $SrRu_{1-x}Cr_xO_3$, showing the boundaries between the perovskite superstructure types. The broken line shows the linear variation expected for $SrRu^{4+}_{1-x}Cr^{4+}_xO_3$ with no charge transfer, and the full line is for the $Ru^{4+}+Cr^{4+} \rightarrow Ru^{5+}+Cr^{3+}$ charge transfer model described in the text.

No x-ray diffraction evidence for Cr/Ru cation ordering is observed in our $SrRu_{1-x}Cr_xO_3$ samples at any x and so the volume would be expected to vary linearly with x. However, the experimental variation in Fig. 10 shows two essentially linear regions that meet near $x=0.5$. This discontinuity is not associated with the above changes of superstructure symmetry, but is consistent with the size changes expected from Ru^{4+} (0.62 Å)$+Cr^{4+}$ (0.55 Å)$\rightarrow Ru^{5+}$ (0.565 Å) $+Cr^{3+}$ (0.615 Å) charge transfer. From the ionic radii[13] (shown in parenthesis) an expansion of 0.01 Å is predicted per electron transfer. If a full transfer occurs then the formal valence distribution varies with x as $SrRu^{4+}_{1-2x}Ru^{5+}_xCr^{3+}_xO_3$ for $0<x<0.5$ and $SrRu^{5+}_{1-x}Cr^{3+}_{1-x}Cr^{4+}_{2x-1}O_3$ for $0.5<x<1$, and so linear variations of volume are expected in each regime, with a discontinuity at $x=0.5$. A fit of two linear regions for charge transfer is shown in Fig. 10. From this, the ratio a_{53}/a_{44} is found to be 1.0044, where a_{53} is the cubic unit cell parameter for a fully charge transferred $SrRu^{5+}_{0.5}Cr^{3+}_{0.5}O_3$ solid solution, and a_{44} is for $SrRu^{4+}_{0.5}Cr^{4+}_{0.5}O_3$ with no charge transfer. Using tabulated ionic radii, a_{53}/a_{44} is estimated to be 1.0025; the difference between this and the experimental value is within the error limits of the reported ionic radii (typically ±0.025 Å). Hence, the observed volume variation in the $SrRu_{1-x}Cr_xO_3$ system is consistent with an essentially complete $Ru^{4+}+Cr^{4+} \rightarrow Ru^{5+}+Cr^{3+}$ charge transfer. The increase in T_c with Cr doping, whereas other substitutions into $SrRuO_3$ suppress T_c, also provides evidence for charge transfer that enhances ferromagnetism through a double exchange interaction, as noted previously.[8]

Although both $SrRuO_3$ and $SrCrO_3$ are metallic, resistivity measurements (Fig. 1) show that intermediate $SrRu_{1-x}Cr_xO_3$ solid solutions are insulating for $x=0.4$–0.6. The mixing of Cr and Ru provides two mechanisms that may lead to this electron localization. The disorder created by the random cation substitutions tends to localize carriers and eventually induces an Anderson transition to an insulating state. In addition, the above $Ru^{4+}(t^4_{2g})+Cr^{4+}(t^2_{2g}) \rightarrow Ru^{5+}(t^3_{2g})+Cr^{3+}(t^3_{2g})$ charge transfer eliminates the charge carriers in both bands (minority-spin t_{2g} electrons in Ru^{4+} bands and the holes in the majority-spin t_{2g} band of Cr^{4+}) leading to insulating behavior around x=0.5.

There are two metal-insulator transitions in the $SrRu_{1-x}Cr_xO_3$ system, at approximately $x=0.3$ and 0.7 (Fig. 11). The low x transition is between the metallic, orthorhombic *Pbnm* $SrRuO_3$-type phase, which becomes a band ferromagnet at low temperatures, and the insulating, rhombohedral $R\bar{3}c$ phase which orders antiferromagnetically with a high T_N. The metal-insulator, magnetic, and structural transitions appear to be coincident, but further work will be needed to test this over smaller composition intervals. There is no symmetry group-subgroup relation between the *Pbnm* and $R\bar{3}c$ perovskite superstructures, and so the transition is first order and can lead to two-phase coexistence regions. The broad ferromagnetic ordering seen in the magnetization curve for $SrRu_{0.6}Cr_{0.4}O_3$ suggests that some orthorhombic phase is also present, although this is not seen in the neutron

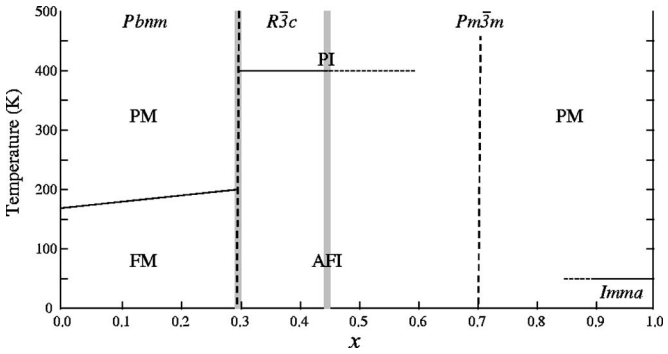

FIG. 11. A schematic phase diagram for the $SrRu_{1-x}Cr_xO_3$ system based on the present results. Phase labels; P/F/AF = para/ferro/antiferromagnetic; M/I metallic/insulating. Approximate superstructure and metal-insulator transitions are shown as grey and broken lines, respectively.

diffraction profiles. The first order $R\bar{3}c \rightarrow Pbnm$ structural transition can be chemically tuned to coincide with the metal-insulator transition in the manganite $La_{0.83}Sr_{0.17}MnO_3$, leading to large magnetostructural couplings,[14] and similar phenomena may be accessible in the $SrRu_{1-x}Cr_xO_3$ system close to the $x=0.3$ transition.

The other metal-insulator transition occurs in the cubic regime near $x=0.7$, without a change of symmetry. The anomalously high value of the volume at $x=0.6$ (Fig. 10) could signify some electron-lattice coupling in proximity to this transition. The metallic phase appears to be Pauli paramagnetic down to 4 K, with the apparent 190 K ferromagnetism [Fig. 8(a)] resulting from a trace of the low x orthorhombic phase.

V. CONCLUSIONS

This study has revealed that an entire range of $SrRu_{1-x}Cr_xO_3$ perovskite solid solutions can be prepared using high temperatures and pressures. A substantial $Ru^{4+}+Cr^{4+} \rightarrow Ru^{5+}+Cr^{3+}$ charge transfer is evidenced by a volume-composition discontinuity near $x=0.5$, as well as by enhancement of the ferromagnetic transition at low x. Three distinct electronic regimes are found. Low Cr-doped materials ($x<0.3$) are itinerant-electron ferromagnets with an orthorhombic *Pbnm* perovskite superstructure, as in $SrRuO_3$, and show an enhancement of T_c from 160 to 190 K due to an additional Cr^{3+}/Cr^{4+} double exchange. An insulating region is found for $0.3<x<0.7$ in which both rhombohedral and cubic structural phases occur. Antiferromagnetic *G*-type order with a high Néel temperature ($\sim$400 K) is found for the rhombohedral $x=0.4$ phase. $0.7<x<1$ samples are cubic and Pauli paramagnetic, as typified by $SrCrO_3$. However, low-temperature magnetic and structural transitions indicate that the ground state of $SrCrO_3$ is more subtle than previously reported, with a possible weak ferromagnetism arising from modifications of the Fermi surface. Further work is needed to clarify the nature of these correlated-electron states, and to investigate the phenomena that may arise from phase co-existence or competition at the structural, magnetic, and electronic phase boundaries.

ACKNOWLEDGMENTS

We thank EPSRC for the provision of neutron beam time at ISIS and ILL, P. Radaelli (ISIS), and P. Henry (ILL) for assistance with data collection, and W. Schnick for support of the studies at LMU. Funding through ESF COST network D30/003/03 and CICyT (Spain) through Project No. MAT2004-0479 is also acknowledged.

[1] J. M. Longo, P. M. Raccah, and J. B. Goodenough, J. Appl. Phys. **39**, 1327 (1968).
[2] L. Klein, J. S. Dodge, C. H. Ahn, J. W. Reiner, L. Mieville, T. H. Geballe, M. R. Beasley, and A. Kapitulnik, J. Phys.: Condens. Matter **8**, 10111 (1996).
[3] I. I. Mazin and D. J. Singh, Phys. Rev. B **56**, 2556 (1997).
[4] G. Cao, S. McCall, M. Shepard, J. E. Crow, and R. P. Guertin, Phys. Rev. B **56**, 321 (1997).
[5] B. L. Chamberlands, Solid State Commun. **5**, 663 (1967).
[6] L. Pi, A. Maignan, R. Retoux, and B. Raveau, J. Phys.: Condens. Matter **14**, 7391 (2002).
[7] Z. H. Han, J. I. Budnick, W. A. Hines, B. Dabrowski, S. Kolesnik, and T. Maxwell, J. Phys.: Condens. Matter **17**, 1193 (2005).
[8] B. Dabrowski, S. Kolesnik, O. Chmaissem, T. Maxwell, M. Avdeev, P. W. Barnes, and J. D. Jorgensen, Phys. Rev. B **72**, 054428 (2005).
[9] H. Huppertz, Z. Kristallogr. **219**, 330 (2004).
[10] L. M. Rodriguez-Martinez and J. P. Attfield, Phys. Rev. B **63**, 024424 (2001).
[11] A. C. Larson and R. B. Von Dreele, General Structure Analysis System, Los Alamos National Laboratory, Report No. LAUR 86-748, 1994 (unpublished).
[12] K. I. Kobayashi, T. Kimora, H. Sawada, K. Terakura, and Y. Tokura, Nature (London) **395**, 677 (1998).
[13] R. D. Shannon, Acta Crystallogr., Sect. A: Cryst. Phys., Diffr., Theor. Gen. Crystallogr. **A32**, 751 (1976).
[14] A. Asamitsu, Y. Moritomo, Y. Tomioka, T. Arima, and Y. Tokura, Nature (London) **373**, 407 (1995).